Comparison of the random-phase approximation with the multichannel frozen-core Hartree-Fock approximation for the photoionization of N_2

Robert R. Lucchese and Robert W. Zurales
Department of Chemistry, Texas A&M University, College Station, Texas 77843
(Received 10 December 1990)

The photoionization of N_2 leading to the $X\,^2\Sigma_g^+$, $A\,^2\Pi_u$, and $B\,^2\Sigma_u^+$ states of N_2^+ has been studied using the random-phase approximation (RPA) and the multichannel frozen-core Hartree-Fock (MCFCHF) approximation. The RPA has been implemented as a coupled-channel method with a set of open and closed channels corresponding to excitation operators and with a set of closed channels corresponding to deexcitation operators. Thus in the case of the photoionization of N_2 there are 14 coupled channels. Both the RPA and MCFCHF were solved using the Schwinger variational method with Padé-approximant corrections. Good agreement was found between the RPA results and the MCFCHF results when the dipole-mixed form of the cross section was used. In comparison with experiment, both of these methods show qualitative improvements over previous computational results. These calculations give the correct behavior of the cross section in the $1\pi_u \rightarrow k\pi_g$ channel without *ad hoc* corrections needed in earlier calculations. Also both of these methods exhibit autoionizing resonances lacking in earlier results. However, there are still a number of discrepancies between theory and experiment, including the position and shape of the autoionization resonances, and the behavior of the photoelectron asymmetry parameters in the $(2\sigma_u)^{-1}$ ionization channel, which is strongly perturbed by the shape resonance in the $(3\sigma_g)^{-1}$ ionization channel.

I. INTRODUCTION

The photoionization of N_2 has been studied by numerous theoretical methods [1–7] and also has been the object of many experimental studies [8–11]. This system is a prototype of molecular photoionization with three characteristics: It is a highly anisotropic system, it has both one-particle (shape resonances) and two-particle (autoionization) resonances, and it also has a vibrational mode. Additionally, N_2 is an important atmospheric molecule. Here we will consider the photoionization process in the fixed-nuclei approximation, and we will limit ourselves to consider only the ionization from the valence orbitals on N_2. With these restrictions we will consider the effects of electron correlation on the total and differential cross sections leading to the $X\,^2\Sigma_g^+$, $A\,^2\Pi_u$, and $B\,^2\Sigma_u^+$ states of N_2^+.

There are three questions in particular which we will examine. The first question is what degree of correlation is needed to accurately treat the $1\pi_u \rightarrow k\pi_g$ channel. In the separated-channel frozen-core Hartree-Fock (SCFCHF) approximation there is a strong valence transition in this channel which appears above threshold. In previous studies [2,12], the interaction potential for this channel was modified to remove this state. Although this procedure leads to more reasonable predictions for the cross sections, its *ad hoc* nature keeps the method from being a generally applicable approach. The second question is what degree of correlation is needed to accurately describe the effects of interchannel coupling on the photoelectron asymmetry parameters in the $(2\sigma_u)^{-1}$ channel [1,10], which are greatly affected by the shape resonance in the $(3\sigma_g)^{-1}$ channel. Finally, we will consider how well the position and widths of the autoionization states leading up to the $(2\sigma_u)^{-1}$ threshold are predicted at the level of theory considered here.

In the present study we have considered two alternative approaches for including electron correlation in the computation of the photoionization cross sections of N_2. We have computed the photoionization cross section using the multichannel frozen-core Hartree-Fock (MCFCHF) [1,13] method and the random-phase approximation (RPA) [14]. Both of these methods can be cast as sets of close-coupled equations involving nonlocal nonspherically symmetric coupling potentials [15]. In the case of the MCFCHF calculations, the four valence ion states were included in the calculation. In the RPA calculations all 14 channels were included, where seven of the channels correspond to excitation operators and seven of the channels to deexcitation operators. Once these methods are written in the form of close-coupled equations, the resulting equations were then solved using the Schwinger variational method with Padé-approximant corrections [16]. All of the required matrix elements were computed using single-center expansion techniques [16,17].

Both the MCFCHF and the RPA methods have been applied to the photoionization of N_2 previously. In earlier two-channel MCFCHF calculations [1,18] the vibrational branching ratios and the fixed-nuclei results were obtained. However, these results do not give quantitative agreement with available experimental data [10]. The RPA method has been previously applied [5–7] to the photoionization of N_2. However, these studies used basis-function methods which did not give angular distributions and which required additional approximations to

obtain partial channel cross sections. In this paper we will only compare our current results to those of Swanstrøm *et al.* [5] since those authors did obtain approximate partial channel results and they considered all of the relevant channels.

In addition to RPA cross sections, Swanstrøm *et al.* [5] also computed *multiconfigurational* RPA (MCRPA) cross sections for the photoionization of N_2. In the MCRPA calculations of Swanstrøm *et al.* [5] the initial state was treated using a multiconfigurational wave function, and appropriate transfer operators were then added to the operator basis set. Unfortunately, the acronym MCRPA has also been used by Cacelli and co-workers [19,20] to denote *multichannel* RPA. A multichannel RPA is an RPA calculation where all channel couplings are included but where the target states are represented by frozen-core Hartree-Fock (FCHF) wave functions. The calculations presented in this study are multichannel RPA calculations (which we will denote by just RPA) but they are not MCRPA calculations using the definition of Swanstrøm *et al.* [5].

In the energy region of the Hopfield autoionization series leading up to the $B\,^2\Sigma_u^+$ threshold, we will also compare our results to those obtained by Raoult *et al.* [3] who used the multichannel quantum-defect theory (MQDT). In their calculations, the parameters used in the MQDT were obtained from a SCFCHF calculation. These MQDT results can thus be characterized as distorted-wave calculations, where the effects of channel coupling are only included to first order.

II. THEORY

The basic scattering equations that describe the final state of the photoionization process can be written using a scattering wave function for an N-electron system of the form [21]

$$\Psi_S = \sum_\lambda A\,\theta_\lambda P \psi_{\lambda S} \tag{1}$$

where A is an N-electron antisymmetrization operator, and θ_λ are $(N-1)$-electron target states. The projection operator P enforces orthogonality between the orbitals $\psi_{\lambda S}$ and all of the bound orbitals used to describe the target states θ_λ. Thus P is a one-electron operator of the form

$$P = 1 - \sum_i |\phi_i\rangle\langle\phi_i| \ , \tag{2}$$

where the orbitals $|\phi_i\rangle$ are the bound orbitals used to describe the target. The appropriate Lippmann-Schwinger equation for the scattering functions $\psi_{\lambda S}$ can then be obtained from the Schrödinger equation by projecting onto the subspace spanned by the scattering function. This leads to an equation of the form

$$\boldsymbol{\psi}_S = \boldsymbol{\phi}_S + \underline{G}\,\underline{V}\boldsymbol{\psi}_S \ , \tag{3}$$

where $\boldsymbol{\psi}_S$ is a vector of the channel solutions, $\boldsymbol{\phi}_S$ is a vector of the homogeneous solutions (i.e., in the absence of $\underline{V}$), $\underline{V}$ is the optical potential matrix which can be written (in atomic units) as [21,22]

$$\underline{V} = \underline{P}\langle\theta|H-E|A^2\theta^T\rangle_{N-1}\underline{P} + \left[\frac{1}{2}\nabla^2 + \frac{1}{r} + \underline{\tilde{E}}\right] . \tag{4}$$

θ is a vector of target states, the superscript T indicates the transpose, the subscript $N-1$ indicates integration over $N-1$ electronic coordinates, $\underline{P}$ is a matrix defined by $(\underline{P})_{ij} = \delta_{ij}P$, $\underline{\tilde{E}}$ is defined by $(\underline{\tilde{E}})_{ij} = \delta_{ij}E_i$, where E_i is the asymptotic energy of the electron leaving the system in target state θ_i, and where $\underline{G}$ is the matrix of Coulomb channel Green's functions defined by $(\underline{G})_{ij} = \delta_{ij}G(E_i)$. The kernel of the Coulomb channel Green's function satisfies the equation

$$\left[-\frac{1}{2}\nabla^2 - \frac{1}{r} - E_i\right] G(\mathbf{r},\mathbf{r}') = -\delta^3(\mathbf{r}-\mathbf{r}') \ . \tag{5}$$

In the MCFCHF approximation the optical potential $\underline{V}$ given in Eq. (4) has the form of a Phillips-Kleinman (PK) pseudopotential [2,23]:

$$\underline{V}^{\mathrm{MCPK}} = \underline{V}^{\mathrm{HF}} + \underline{V}^{C} - \underline{L}\underline{Q} - \underline{Q}\underline{L} + \underline{Q}\underline{L}\underline{Q} \ , \tag{6}$$

where $\underline{L}$, $\underline{Q}$, and $\underline{V}^{\mathrm{HF}}$ are defined by

$$(\underline{L})_{pq} = \left[-\frac{1}{2}\nabla^2 - \frac{1}{r} + E_p\right]\delta_{pq} + (\underline{V}^{\mathrm{HF}})_{pq} + (\underline{V}^{C})_{pq} \ , \tag{7}$$

$$(\underline{Q})_{pq} = \left[\sum_{S=1}^{n} |\phi_S\rangle\langle\psi_S|\right]\delta_{pq} \ , \tag{8}$$

$$(\underline{V}^{\mathrm{HF}})_{pq} = \left[-\sum_\alpha \frac{Z_\alpha}{r_\alpha} + \frac{1}{r} + \sum_{t=1}^{n}(2J_{tt} - K_{tt})\right]\delta_{pq} \ , \tag{9}$$

and

$$(\underline{V}^{C})_{pq} = -J_{t_p t_q} + 2K_{t_p t_q} \ . \tag{10}$$

In Eqs. (7)–(10) n is the number of occupied orbitals, the sum over α runs over the nuclei, the index t_p indicates the orbital from which an electron is removed to give the ionic state in channel p, and J and K are Coulomb and exchange integrals.

An alternative approach to obtaining a set of scattering equations which include correlation effects is through the RPA or related formulations [14]. For the study of photoionization cross sections we have implemented the multichannel RPA by rewriting the usual matrix RPA equations as a set of close-coupling equations which have the same form as those given in Eq. (3). In the RPA, an excitation operator $A^\dagger$ is defined by

$$A^\dagger(E)|0\rangle = |E\rangle \tag{11}$$

and

$$[H, A^\dagger(E)]|0\rangle = \Delta E|E\rangle \ , \tag{12}$$

where $|0\rangle$ is the ground state with energy E_0, $|E\rangle$ is an excited state with energy E, and $\Delta E = E - E_0$. By expanding $A^\dagger(E)$ in single particle-hole excitation and deexcitation operators and linearizing the resulting equations, where $|0\rangle$ is a closed-shell singlet Hartree-Fock (HF) wave function with n occupied orbitals indexed by α

and β and where $|E\rangle$ is a singlet state, a set of integrodifferential equations is obtained of the form [7,15]

$$0=P(H^{\mathrm{HF}}-\varepsilon_\alpha-\Delta E)PY_\alpha(\mathbf{r}) + \sum_\beta P(2K_{\beta\alpha}-J_{\beta\alpha})PY_\beta(\mathbf{r}) + \sum_\beta P(2I_{\beta\alpha}-I_{\alpha\beta})\tilde{P}Z_\beta(\mathbf{r}) \quad (13)$$

and

$$0=\tilde{P}(\tilde{H}^{\mathrm{HF}}-\varepsilon_\alpha+\Delta E)\tilde{P}Z_\alpha(\mathbf{r}) + \sum_\beta \tilde{P}(2\tilde{K}_{\beta\alpha}-\tilde{J}_{\beta\alpha})\tilde{P}Z_\beta(\mathbf{r}) + \sum_\beta \tilde{P}(2\tilde{I}_{\beta\alpha}-\tilde{I}_{\alpha\beta})PY_\beta(\mathbf{r}) . \quad (14)$$

In Eqs. (13) and (14), H^{HF} is the Hartree-Fock Hamiltonian, ε_i is the orbital eigenvalue of orbital ϕ_i, $J_{\alpha\beta}$ and $K_{\alpha\beta}$ are the usual Coulomb and exchange operators, P is the projection operator defined in Eq. (2), the kernel of $I_{\alpha\beta}$ is given by

$$I_{\alpha\beta}(\mathbf{r},\mathbf{r}')=\frac{\phi_\alpha(\mathbf{r}')\phi_\beta(\mathbf{r})}{|\mathbf{r}-\mathbf{r}'|} , \quad (15)$$

and the tilde over an operator $\tilde{O}$ indicates that the operator is obtained from the operator O by taking the complex conjugate of the kernel. The value of the matrix element of any one-electron operator μ between $|0\rangle$ and $|E\rangle$ is then given by

$$\langle E|\mu|0\rangle=(2)^{1/2}\int d^3r[\phi_\alpha^*(\mathbf{r})\mu(\mathbf{r})Y_\alpha(\mathbf{r}) + Z_\alpha(\mathbf{r})\mu(\mathbf{r})\phi_\alpha(\mathbf{r})] . \quad (16)$$

The RPA equations (13) and (14) can be written in the form of the Lippmann-Schwinger equation given in Eq. (3), where the potential is again a Phillips-Kleinman pseudopotential in the same manner as in the MCFCHF case. The RPA potential $\underline{V}^{\mathrm{RPA}}$ is then a $2n\times 2n$ (n is the number of occupied orbitals in the reference state) matrix given by

$$\underline{V}^{\mathrm{RPA}}=\begin{bmatrix} \underline{V}^{\mathrm{MCPK}} & \underline{V}^{IPK} \\ \tilde{\underline{V}}^{IPK} & \tilde{\underline{V}}^{\mathrm{MCPK}} \end{bmatrix} . \quad (17)$$

where the first n indices refer to the excitation channels, the second n indices refer to the deexcitation channels, and where the $\underline{V}^{\mathrm{MCPK}}$ matrix is the same as given in Eq. (6) with all n possible channels included. In the RPA formulation, the channel energies in the excitation channels are $E_i=E-E_0+\varepsilon_i$ and the channel energies in the deexcitation channels are $E_i=-E+E_0+\varepsilon_i$. As before, the tilde over an operator implies that the kernel of any integral operator contained in that operator is complex conjugated. In Eq. (17), the potential $\underline{V}^{IPK}$ is defined by

$$\underline{V}^{IPK}=\underline{V}^I-\underline{V}^I\underline{\tilde{Q}}-\underline{Q}\underline{V}^I+\underline{Q}\underline{V}^I\underline{\tilde{Q}} , \quad (18)$$

where

$$(\underline{V}^I)_{\alpha\beta}=2I_{\beta\alpha}-I_{\alpha\beta} . \quad (19)$$

Note that using this multichannel formulation, both the MCFCHF and the RPA calculations naturally include both one-electron shape resonances found in separated-channel calculations and two-electron autoionization resonances. As the photon energy E is lowered below a given threshold $E_0-\varepsilon_i$, the channel energy E_i becomes negative. Then the channel Green's function that is used is that appropriate for a closed channel. The states which would be bound states of the closed channel in a separated-channel approximation become autoionizing states in the coupled-channel problem.

In this study of photoionization, we do not need to directly compute the solutions to the Lippmann-Schwinger equation given in Eq. (3), we only need to compute matrix elements of one-electron operators between the HF initial state and the multichannel final-state wave function. To compute these matrix elements we use the $\tilde{C}$-functional variational method with Padé-approximant corrections to the initial variational estimate [1,16,24,25]. The explicit form of the functional for a matrix element of the operator $\underline{Q}$ is

$$\langle\phi_t|\underline{Q}|\psi_{E\hat{\mathbf{k}}p}^{(-)}\rangle\approx M_{35}^3(\phi_t\underline{Q},\phi_{E\hat{\mathbf{k}}p}^{(-)}) =\langle\phi_t|\underline{Q}|\phi_{E\hat{\mathbf{k}}p}^{(-)}\rangle+\langle\phi_t|\underline{Q}\,\underline{G}_c\underline{V}_Q|\phi_{E\hat{\mathbf{k}}p}^{(-)}\rangle+\langle\phi_t|\underline{Q}\,\underline{G}_c\underline{V}_Q\underline{G}_c\underline{V}_Q|\phi_{E\hat{\mathbf{k}}p}^{(-)}\rangle + \sum_{\alpha,\beta}[\langle\phi_t|\underline{Q}\,\underline{G}_c\underline{V}_Q\underline{G}_c\underline{V}_Q|\alpha\rangle(\underline{D}^{-1})_{\alpha\beta}\langle\beta|\underline{V}_Q\underline{G}_c\underline{V}_Q|\phi_{E\hat{\mathbf{k}}p}^{(-)}\rangle] , \quad (20)$$

where the matrix $\underline{D}$ is given by

$$(\underline{D})_{\alpha\beta}=\langle\alpha|\underline{V}_Q-\underline{V}_Q\underline{G}_c\underline{V}_Q|\beta\rangle , \quad (21)$$

and where $|\alpha\rangle$ and $|\beta\rangle$ are elements of a multichannel square-integrable basis set and $|\phi_t\rangle$ is a vector which contains the orbitals ϕ_{t_p} in the corresponding channels p. An initial estimate of the matrix element of interest is obtained using Eq. (20); then the variational basis is augmented systematically with continuum functions. The sequence of estimates formed in this manner [25] are equivalent to a diagonal $[N/N]$ Padé sequence for the difference in the first variational estimate and the exact matrix element for the given interaction potential $\underline{V}$.

In order to compute both total and differential cross sections for the photoionization by light, which is linearly

polarized in the $\hat{\mathbf{n}}$ direction, dynamical coefficients $I_{E\hat{\mathbf{k}}p\hat{\mathbf{n}}}$ are computed using Eq. (20) in both the length form, using

$$I^L_{E\hat{\mathbf{k}}p\hat{\mathbf{n}}} = (k)^{1/2} \langle \phi_t | \mathbf{r}\cdot\hat{\mathbf{n}} | \psi^{(-)}_{E\hat{\mathbf{k}}p} \rangle \ , \tag{22}$$

and in the velocity form, using

$$I^V_{E\hat{\mathbf{k}}p\hat{\mathbf{n}}} = \frac{(k)^{1/2}}{\hbar\omega} \langle \phi_t | \nabla\cdot\hat{\mathbf{n}} | \psi^{(-)}_{E\hat{\mathbf{k}}p} \rangle \ . \tag{23}$$

We then compute the total and differential cross sections in the mixed form using [26]

$$\frac{d^2\sigma^M_{Ep}}{d\Omega_{\hat{\mathbf{k}}} d\Omega_{\hat{\mathbf{n}}}} = \frac{4\pi^2\hbar\omega}{c} \mathrm{Re}([I^L_{E\hat{\mathbf{k}}p\hat{\mathbf{n}}}]^* I^V_{E\hat{\mathbf{k}}p\hat{\mathbf{n}}}) \ , \tag{24}$$

where $\hbar\omega$ is the energy of the ionizing photon and c is the speed of light. The final cross sections are obtained in the usual manner by integrating over all orientations of the molecule in the laboratory frame to give the differential cross section as [27]

$$\frac{d\sigma^M_{Ep}}{d\Omega_{\hat{\mathbf{k}}}} = \frac{\sigma^M_{Ep}}{4\pi} [1 + \beta_{E_p} P_2(\cos\theta)] \ , \tag{25}$$

where θ is the angle between $\hat{\mathbf{n}}$ and $\hat{\mathbf{k}}$, P_2 is the Legendre polynomial of degree 2, and β_{E_p} is the photoelectron asymmetry parameter. The mixed form of the cross section is believed to be more useful than either the usual length or velocity forms of the cross section, since the oscillator strength computed in the mixed form satisfies the Thomas-Reiche-Kuhn (TRK) sum rule [28].

The Padé sequence method converged very rapidly in this study. In regions where the cross sections were slowly varying functions of the energy, the cross sections changed by less than 1% between the $N=2$ and 3 estimate. In the regions where autoionization was important, we typically needed $N=4$–6 to obtain satisfactory convergence. One advantage of using the Padé approximants is that they can eliminate the spurious singularities which occur with these variational methods when only a single fixed-basis-set calculation is considered [29]. The cross sections in the $3\sigma_g \rightarrow k\sigma_u$ channel are shown in Fig. 1 as obtained using the variational estimate using only the original basis given in Table I (denoted as $N=0$) and using the Padé approximants up to $N=3$. These cross sections were obtained using the four-channel MCFCHF approximation. The spurious structure in the noniterative ($N=0$) result is due to a zero in the determinant of the matrix D at a photon energy of approximately 32 eV. With the iterative method, the effects of this spurious singularity are removed from the computed cross section. Thus, we have found that being able to compute a basis-set-independent result in the Padé-approximant approach can greatly reduce the effort needed to assure the convergence of a calculation in comparison to methods which are strictly dependent on basis sets, such as the multichannel Schwinger method [30] and the complex Kohn method [31].

We had difficulty converging the Padé-approximant sequence at only one energy of the many energies considered in this study. This occurred at $E=34.80$ eV in

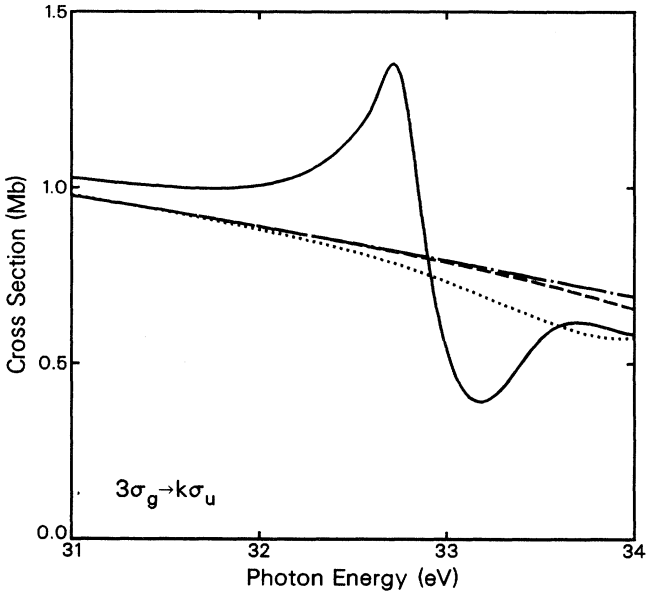

FIG. 1. Convergence of the partial photoionization cross section in the $3\sigma_g \rightarrow k\sigma_u$ ionization channel: ——, $N=0$; · · ·, $N=1$; — — —, $N=2$; —·—·-, $N=3$. The difference between the $N=3$ and $N=4$ calculations is not detectable on the scale used in this figure.

the MCFCHF approximation in the $\Delta m=0$ channels, where numerical inaccuracies in the evaluation of the integrals combined with the inversion of nearly singular matrices lead to a Padé sequence that did not converge. The nature of the problem at this energy can be understood by considering the data given in Table II. Here we have given the partial cross section in the $3\sigma_g \rightarrow k\sigma_u$ channel and the determinant of the matrix D which is inverted in the computation of the Padé correction to the matrix element $I^L_{Elmp\hat{\mathbf{n}}}$, where $l=1$ and $m=0$, and the ionization channel index p corresponds to the $(2\sigma_u)^{-1}$ channel. In all stages of the calculation, where a matrix is inverted, the matrices should be complex symmetric matrices. Due to the finite precision with which our matrix elements are computed, the matrices inverted were not exactly symmetric. To judge the numerical stability of this calculation we have compared the determinant and cross sections obtained when the slightly unsymmetric matrices are used and when we have symmetrized the matrices before every matrix inversion. As can be seen from Table II, the fractional errors in both the determinant and the cross sections are not large for $N \leq 2$. For the original basis set, given in Table I, after $N=2$, the difference between the symmetrized and unsymmetrized calculation grows quickly. We have also considered a modified basis set where the ($\mathbf{A}=0$, $l=1$, $m=0$) functions with exponents $\alpha=11.387$ and 2.254 in the $2\sigma_g \rightarrow k\sigma_u$ channel were changed to a ($\mathbf{A}=0$, $l=1$, $m=0$) function with $\alpha=0.054$ and a ($\mathbf{A}=0$, $l=3$, $m=0$) function with $\alpha=0.177$ in the same channel. We can see that even though the calculation with the original basis set was numerically unstable, the resulting error in

TABLE I. Basis sets used in the evaluation of Eq. (20) for $\Delta m=0$. All scattering basis functions are spherical Gaussian functions of the form given in Eq. (26).

Symmetry	(**A**,l,m)[a]	α
$1\pi_u \rightarrow k\pi_g$	(**R**$_N$,1,1)	16, 8, 4, 2, 1, 0.5, 0.25, 0.125
	(**R**$_N$,2,1), (0,2,1)	1, 0.5, 0.25, 0.125
	(0,4,1)	0.25, 0.125
$3\sigma_g \rightarrow k\sigma_u$	(**R**$_N$,0,0)	16, 8, 4, 2, 1, 0.5, 0.25, 0.125
	(**R**$_N$,1,0), (0,1,0)	1, 0.5, 0.25, 0.125
	(0,3,0)	0.25, 0.125
$2\sigma_u \rightarrow k\sigma_g$	(**R**$_N$,0,0)	16, 8, 4, 2, 1, 0.5, 0.25, 0.125
	(**R**$_N$,1,0), (0,0,0)	1, 0.5, 0.25, 0.125
	(0,2,0)	0.25, 0.125
$2\sigma_g \rightarrow k\sigma_u$	(**R**$_N$,0,0), (**R**$_N$,1,0), (0,1,0)	11.387, 2.254, 0.7, 0.269, 0.117, 0.054
$1\sigma_u \rightarrow k\sigma_g$	(**R**$_N$,0,0), (**R**$_N$,1,0), (0,0,0)	304.287, 60.226, 18.718, 7.202, 3.128, 1.434
$1\sigma_g \rightarrow k\sigma_u$	(**R**$_N$,0,0), (**R**$_N$,1,0), (0,1,0)	304.287, 60.226, 18.718, 7.202, 3.128, 1.434
$k\pi_g \rightarrow 1\pi_u$	(**R**$_N$,1,1), (**R**$_N$,2,1), (0,2,1)	70.834, 12.987, 3.633, 1.248, 0.485, 0.200
$k\sigma_u \rightarrow 3\sigma_g$	(**R**$_N$,0,0), (**R**$_N$,1,0), (0,1,0)	32.005, 6.335, 1.969, 0.757, 0.329, 0.151
$k\sigma_g \rightarrow 2\sigma_u$	(**R**$_N$,0,0), (**R**$_N$,1,0), (0,0,0)	35.015, 6.930, 2.154, 0.829, 0.360, 0.165
$k\sigma_u \rightarrow 2\sigma_g$	(**R**$_N$,0,0), (**R**$_N$,1,0), (0,1,0)	49.261, 9.750, 3.030, 1.166, 0.506, 0.232
$k\sigma_g \rightarrow 1\sigma_u$	(**R**$_N$,0,0), (**R**$_N$,1,0), (0,0,0)	342.255, 67.741, 21.054, 8.100, 3.518, 1.612
$k\sigma_u \rightarrow 1\sigma_g$	(**R**$_N$,0,0), (**R**$_N$,1,0), (0,1,0)	342.255, 67.741, 21.054, 8.100, 3.518, 1.612

[a]The spherical Gaussians were either centered at the nuclei, indicated by **A**=**R**$_N$, or at the bond midpoint, indicated by **A**=0.

the total cross section was less than 2% when compared to the well-converged result obtained using the modified basis set.

One advantage of the RPA form of the photoionization calculation is that it gives cross sections that are identical in length and velocity forms and that satisfy the Thomas-Reiche-Kuhn (TRK) sum rule [14, 28]. In this study, we will compare these accurate RPA results with those obtained from the MCFCHF [1] approach using the mixed form of the matrix element to compute the cross sections and photoelectron angular distributions. The mixed form of the MCFCHF method is known to produce cross sections that satisfy the TRK sum rule [28]. This comparison will then indicate to what extent the RPA equations just provide the correct normalization and to what extent the oscillator strength is redistributed in the RPA. In general we will only present results in the mixed form of the cross section for either RPA, MCFCHF, or SCFCHF calculations since they satisfy the TRK sum rules.

TABLE II. Convergence of the $[N/N]$ Padé-approximant sequence at $E=34.80$ eV in the MCFCHF approximation for the $\Delta m=0$ channels. The original basis set is that given in Table I, and the modified basis set is detailed in the text. The cross section σ is for the $3\sigma_g \rightarrow k\sigma_u$ ionization channel. The values $\Delta\det(D)$ and $\Delta\sigma$ indicate the difference between the symmetrized and unsymmetrized calculations as discussed in the text.

	Original basis set				Modified basis set			
N	$\lvert\det(D)\rvert$	$\lvert\frac{\Delta\det(D)}{\det(D)}\rvert$	σ (Mb)	$\lvert\frac{\Delta\sigma}{\sigma}\rvert$	$\lvert\det(D)\rvert$	$\lvert\frac{\Delta\det(D)}{\det(D)}\rvert$	σ (Mb)	$\lvert\frac{\Delta\sigma}{\sigma}\rvert$
0			1.019 978 2	1.529×10^{-5}			1.128 062 9	2.659×10^{-6}
1	2.003×10^{-2}	6.203×10^{-5}	1.114 892 6	1.866×10^{-5}	3.518×10^{-2}	7.275×10^{-5}	1.229 734 5	4.310×10^{-6}
2	4.054×10^{-5}	8.860×10^{-5}	1.118 090 7	2.120×10^{-5}	3.862×10^{-4}	1.978×10^{-4}	1.184 857 0	1.266×10^{-6}
3	2.185×10^{-9}	1.731×10^{-4}	1.118 205 7	3.255×10^{-5}	1.850×10^{-7}	2.747×10^{-4}	1.182 427 0	1.015×10^{-6}
4	7.703×10^{-15}	2.996×10^{-4}	1.118 286 6	4.748×10^{-5}	4.721×10^{-12}	2.689×10^{-4}	1.182 261 8	1.015×10^{-6}
5	2.436×10^{-20}	3.144×10^{-3}	1.118 254 8	4.266×10^{-5}	6.365×10^{-18}	3.779×10^{-4}	1.182 252 7	1.015×10^{-6}
6	1.198×10^{-28}	1.234	1.114 643 9	5.679×10^{-3}	1.324×10^{-25}	5.856×10^{-4}	1.182 252 6	1.015×10^{-6}
7	3.364×10^{-37}	1.252	1.103 875 5	3.564×10^{-2}				
8	5.454×10^{-46}	3.472	1.139 129 2	5.921×10^{-2}				
9	1.895×10^{-54}	2.345	1.140 213 9	1.562×10^{-2}				
10	7.337×10^{-63}	2.664	1.177 019 0	9.328×10^{-3}				
11	2.231×10^{-71}	1.894	1.197 051 0	1.917×10^{-2}				
12	8.829×10^{-80}	1.973×10^{1}	1.196 029 6	1.680×10^{-2}				

TABLE III. Basis sets used in the evaluation of Eq. (20) for $\Delta m = 1$. All scattering basis functions are spherical Gaussian functions of the form given in Eq. (26).

Symmetry	$(\mathbf{A},l,m)$[a]	α
$1\pi_u \rightarrow k\delta_g$	$(\mathbf{R}_N,2,2)$	16, 8, 4, 2, 1, 0.5, 0.25, 0.125
	$(\mathbf{R}_N,3,2)$, (0,2,2)	1, 0.5, 0.25, 0.125
	(0,4,2)	0.25, 0.125
$1\pi_u \rightarrow k\sigma_g$	$(\mathbf{R}_N,0,0)$	16, 8, 4, 2, 1, 0.5, 0.25, 0.125
	$(\mathbf{R}_N,1,0)$, (0,0,0)	1, 0.5, 0.25, 0.125
	(0,2,0)	0.25, 0.125
$3\sigma_g \rightarrow k\pi_u$	$(\mathbf{R}_N,1,1)$	16, 8, 4, 2, 1, 0.5, 0.25, 0.125
	$(\mathbf{R}_N,2,1)$, (0,1,1)	1, 0.5, 0.25, 0.125
	(0,3,1)	0.25, 0.125
$2\sigma_u \rightarrow k\pi_g$	$(\mathbf{R}_N,1,1)$	16, 8, 4, 2, 1, 0.5, 0.25, 0.125
	$(\mathbf{R}_N,2,1)$,(0,2,1)	1, 0.5, 0.25, 0.125
	(0,4,1)	0.25, 0.125
$2\sigma_g \rightarrow k\pi_u$	$(\mathbf{R}_N,1,1)$, $(\mathbf{R}_N,2,1)$, (0,1,1)	11.387, 2.254, 0.7, 0.269, 0.117, 0.054
$1\sigma_u \rightarrow k\pi_g$	$(\mathbf{R}_N,1,1)$, $(\mathbf{R}_N,2,1)$, (0,2,1)	304.287, 60.226, 18.718, 7.202, 3.128, 1.434
$1\sigma_g \rightarrow k\pi_u$	$(\mathbf{R}_N,1,1)$, $(\mathbf{R}_N,2,1)$, (0,1,1)	304.287, 60.226, 18.718, 7.202, 3.128, 1.434
$k\sigma_g \rightarrow 1\pi_u$	$(\mathbf{R}_N,0,0)$, $(\mathbf{R}_N,1,0)$, (0,0,0)	70.834, 12.987, 3.633, 1.248, 0.485, 0.200
$k\delta_g \rightarrow 1\pi_u$	$(\mathbf{R}_N,2,2)$, $(\mathbf{R}_N,3,2)$, (0,2,2)	31.606, 6.256, 1.944, 0.748, 0.325, 0.149
$k\pi_u \rightarrow 3\sigma_g$	$(\mathbf{R}_N,1,1)$, $(\mathbf{R}_N,2,1)$, (0,1,1)	32.005, 6.335, 1.969, 0.757, 0.329, 0.151
$k\pi_g \rightarrow 2\sigma_u$	$(\mathbf{R}_N,1,1)$, $(\mathbf{R}_N,2,1)$, (0,2,1)	35.015, 6.930, 2.154, 0.829, 0.360, 0.165
$k\pi_u \rightarrow 2\sigma_g$	$(\mathbf{R}_N,1,1)$, $(\mathbf{R}_N,2,1)$, (0,1,1)	49.261, 9.750, 3.030, 1.166, 0.506, 0.232
$k\pi_g \rightarrow 1\sigma_u$	$(\mathbf{R}_N,1,1)$, $(\mathbf{R}_N,2,1)$, (0,2,1)	342.255, 67.741, 21.054, 8.100, 3.518, 1.612
$k\pi_u \rightarrow 1\sigma_g$	$(\mathbf{R}_N,1,1)$, $(\mathbf{R}_N,2,1)$, (0,1,1)	342.255, 67.741, 21.054, 8.100, 3.518, 1.612

[a]The spherical Gaussians were either centered at the nuclei, indicated by $\mathbf{A}=\mathbf{R}_N$, or at the bond midpoint, indicated by $\mathbf{A}=0$.

The matrix elements needed to evaluate the variational expressions of the form given in Eq. (20) were computed using numerical techniques based on single-center expansions that have been discussed in detail elsewhere [16, 17]. Here we will only give sufficient details to define our calculation. The radial grid used to study the photoionization of N_2 contained 1584 points and extended to a distance of 175 a.u. The N atoms were located at 1.034 a.u. from the origin. The grid was selected using an automatic-grid-generation algorithm, which will be described elsewhere [32]. In the region near the nuclei, the step size was 0.000 236 a.u. The step size increased at larger distances from the origin up to a value 0.1257 a.u. at the end of the grid.

The integration formulas used for radial integrals on this grid were Newton-Cotes-type formulas [17] that allow for the accurate integration of functions which have discontinuities in their slopes such as occur in the integration of the Coulomb Green's function and in the integration of $1/r_{12}$. The eighth-order integration rule was used for all integration regions. However, at high ls in regions near the origin, this integration scheme is known to be unstable [17], and in these regions a second-order integration rule (i.e., Simpson's rule) was used.

The partial-wave expansions used in this study were as follows: $l_m=60$, where l_m is the maximum l included in the expansion of the scattering functions at all times and is the maximum l included in the expansion of the target orbitals at all times; $\lambda_m=120$, where λ_m is the maximum l included in the expansion of $1/r_{12}$ in both the exchange and static potential terms; and $l_p=11$ for the $\Delta m=0$ channels ($1\pi_u \rightarrow k\pi_g$, $3\sigma_g \rightarrow k\sigma_u$, and $2\sigma_u \rightarrow k\sigma_g$), and $l_p=8$ for the $\Delta m=1$ channels ($1\pi_u \rightarrow k\delta_g$, $1\pi_u \rightarrow k\sigma_g$, $3\sigma_g \rightarrow k\pi_u$, and $2\sigma_u \rightarrow k\pi_g$), where l_p is maximum l included in the expansion of the homogeneous solutions $\phi^{(-)}_{E\hat{\mathbf{k}}p}$.

Tables I and III give the initial variational scattering basis set used to evaluate Eq. (20). The variational functions $|\alpha\rangle$ are zero in each channel except for one channel in which there is a spherical Gaussian function of the form

$$\phi^{\alpha,l,m,\mathbf{A}}(\mathbf{r})=N|\mathbf{r}-\mathbf{A}|\exp(-\alpha|\mathbf{r}-\mathbf{A}|^2)Y_{lm}(\Omega_{\mathbf{r}-\mathbf{A}}) , \tag{26}$$

where $\mathbf{A}$ is the center of the function and N is a normalization constant. The use of reasonably large basis sets is essential for the Padé sequence to converge rapidly.

The HF wave function for the initial state of N_2 was constructed from a one-electron basis set which was composed of the primitive Gaussians used by Rizzo, Graham, and Yeager [33], where the primitive functions were not contracted, additional uncontracted s Gaussians with exponents 0.0512, 0.0197, p Gaussians with exponents 0.0416 and 0.0166, and a d Gaussian with exponent 0.1. With a R(N—N) bond distance of 2.068 a.u., the total HF energy was $E=-108.991\,48$ a.u.

III. RESULTS AND DISCUSSION

We have considered the photoionization of N_2 leading to the three lowest states of N_2^+. These states are [34]

the $(3\sigma_g)^{-1}$ $X\,^2\Sigma_g^+$ state which has an experimental ionization potential (IP) of 15.58 eV, the $(2\pi_u)^{-1}$ $A\,^2\Pi_u$ state which has an experimental IP of 16.70 eV, and the $(2\sigma_u)^{-1}$ $B\,^2\Sigma_u^+$ state which has an experimental IP of 18.75 eV. In the MCFCHF calculations, we have considered the interactions between these three channels, and we have included the $(2\sigma_g)^{-1}$ ionization channel so that four electronic states were included in the calculation. We have used the experimental values of the IP's for the thresholds for each of the channels. For $(2\sigma_g)^{-1}$ we have used the value of 37.9 eV [34]. It is well known that the actual states of N_2^+ in the energy of the $(2\sigma_g)^{-1}$ threshold region are not well described by the simple single-configuration hole states implied in the frozen-core approximation [35, 36]. Thus the resonance structure in the photoionization cross section, which results from the inclusion of the $(2\sigma_g)^{-1}$ channel, will not quantitatively reproduce the structure that would be obtained if more accurate states of the N_2^+ system were used. However, the $(2\sigma_g)^{-1}$ target state can be thought of as a polarization pseudostate which provides for the polarization of the other target states [21]. We then expect that at photon energies where there are no resonant states, effects of accurate $(2\sigma_g)^{-1}$ hole states would be similar to those found in this calculation. We additionally note that the $(2\sigma_g)^{-1}$ state is the only low-lying pseudostate that can directly contribute to the photoionization cross section within the FCHF approximation used to describe the ion states. Thus the results obtained with the simple FCHF $(2\sigma_g)^{-1}$ hole states should qualitatively predict the effects of the innervalence hole states of N_2^+ on the photoionization cross sections of N_2.

In the RPA calculations, the channel thresholds are Koopmans' theorem values. Thus the RPA thresholds were 426.75 eV for the $(1\sigma_g)^{-1}$ channel, 426.65 eV for the $(1\sigma_u)^{-1}$ channel, 40.11 eV for the $(2\sigma_g)^{-1}$ channel, 21.18 eV for the $(2\sigma_u)^{-1}$ channel, 16.75 eV for the $(1\pi_u)^{-1}$ channel, and 17.28 eV for the $(3\sigma_g)^{-1}$ channel. Due to the difference between the RPA thresholds and the experimental thresholds, we have not attempted to use the RPA to study the autoionization resonances, which occur just below these thresholds.

In Fig. 2 we present a comparison of the different forms of the photoionization cross section for the MCFCHF and RPA calculations for the $(1\pi_u)^{-1}$ ionization channel. We can see that in the MCFCHF results there is a large difference between the length and velocity forms of the cross section. This indicates that there are significant correlation errors in this calculation. However, the mixed form of the cross section is in relatively good agreement with the RPA calculation. The RPA calculations presented in Fig. 2 show that length and velocity are in very good agreement. In order to obtain this level of agreement between the RPA length and velocity cross sections, we were forced to use a very large basis set to describe the target wave function, as discussed above, and we needed to extend the partial-wave expansions to much higher l than we had previously used [2] in studies of the photoionization of N_2. In Fig. 3 we compare the mixed form of the SCFCHF, MCFCHF, and RPA calculations with available experimental data of Hamnett,

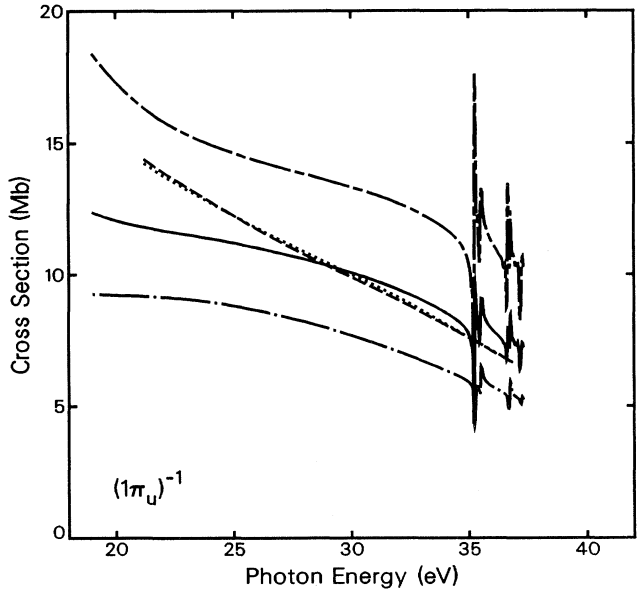

FIG. 2. Photoionization cross section in the $(1\pi_u)^{-1}$ channel. Length, mixed, and velocity forms for the four channel MCFCHF and RPA calculations: — — —, RPA length form; · · ·, RPA velocity form; —·—·—, MCFCHF four-channel length form; —·—·—·—, MCFCHF four-channel velocity form; ——, MCFCHF four-channel mixed form.

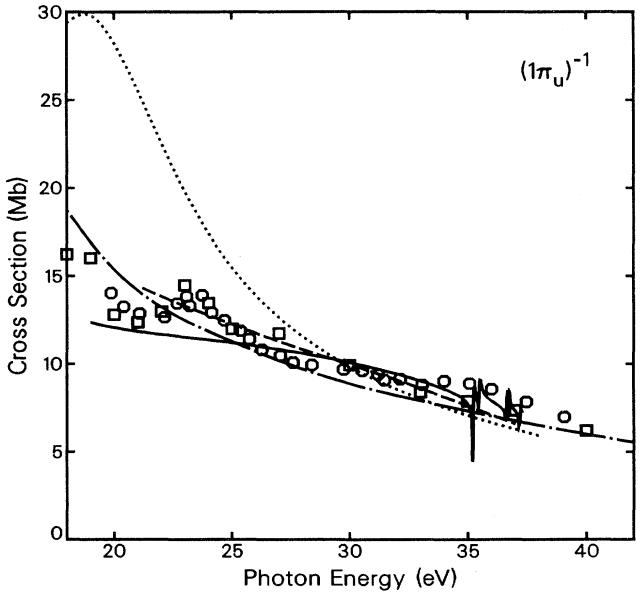

FIG. 3. Photoionization cross section in the $(1\pi_u)^{-1}$ channel. Mixed form for the SCFCHF, four-channel MCFCHF, and RPA calculations with comparison to experiment: ——, MCFCHF four-channel mixed form; — — —, RPA mixed form; · · ·, SCFCHF mixed form; —·—·—·—, RPA results of Swanstrøm *et al.* [5]; □, experimental data from Hamnett, Stoll, and Brion [8]; ○, experimental data of Plummer *et al.* [9].

Stoll, and Brion [8] and Plummer *et al.* [9] and with previous RPA calculations of Swanstrøm *et al.* [5]. In the SCFCHF approximation there is a large peak at threshold due to oscillator strength in the $1\pi_u \rightarrow k\pi_g$ channel. We can see that the correlation induced in the MCFCHF calculation leads to much better agreement with the experimental data and that for this channel, the RPA and MCFCHF results are of similar quality. The present RPA results are also in reasonable agreement with the RPA results of Swanstrøm *et al.* [5].

In the figures where we present cross sections and asymmetry parameters for the MCFCHF calculations, we have carefully computed enough points to obtain any structure at an energy resolution of 0.05 eV. Thus we have not attempted to compute cross sections within 0.6 eV of a new threshold since it would be difficult to resolve all of the structures in these regions. In the RPA results we have not attempted to study the cross sections in the region where autoionization occurs. We did this since the thresholds are at the wrong energies in the RPA. We could have shifted the thresholds, but such a procedure would have had no theoretical justification, and the result would have been no more useful than the MCFCHF results which we present here.

In Fig. 4 we present the photoelectron asymmetry parameters for ionization in the $(1\pi_u)^{-1}$ channel. The RPA and MCFCHF results are nearly identical for this quantity. The only difference being the presence of the autoionization resonances in the MCFCHF results below 37.9 eV. There is reasonable agreement between the theoretical values for the asymmetry parameters and the experimental data of Marr *et al.* [37]. The multichannel theory is in somewhat better agreement with the experiment than is the separated-channel theory. However, when a modified potential was used in the SCFCHF calculation [2] that removed the $1\pi_u \rightarrow k\pi_g$ intensity, the agreement between the SCFCHF results and the experiment was comparable to that found with the present MCFCHF results.

The $(3\sigma_g)^{-1}$ ionization channel contains a shape resonance which is the broad feature centered around 32 eV seen in Fig. 5. It is evident from Fig. 5 that the SCFCHF results are in better agreement with the experimental data of Hamnett, Stoll, and Brion [8] and of Plummer *et al.* [9] at high energies than are the more sophisticated MCFCHF and RPA calculations. In the region of the shape resonance, the interchannel coupling has somewhat broadened the resonance and shifted it to higher energy. By comparison to earlier two-channel MCFCHF calculations [1,18] (not shown), which only included coupling between the $(3\sigma_g)^{-1}$ and $(2\sigma_u)^{-1}$ channels and which did not substantially affect this resonance, we can conclude that the coupling to the $(1\pi_u)^{-1}$ channel is probably responsible for these modifications to the resonant cross section. This conclusion is also supported by the fact that the $3\sigma_g \rightarrow k\sigma_u$ transition is important in correlating the $1\pi_u \rightarrow k\pi_g$ channel [5]. This indicates that further initial and final-state correlations would have to be included for these transitions to be treated in a satisfactory fashion. The investigations of these issues are outside the scope of the current study.

The agreement between the current RPA and the RPA results of Swanstrøm *et al.* [5] shown in Fig. 5 is rather poor. This discrepancy can be attributed to several deficiencies in the earlier calculation: the incompleteness

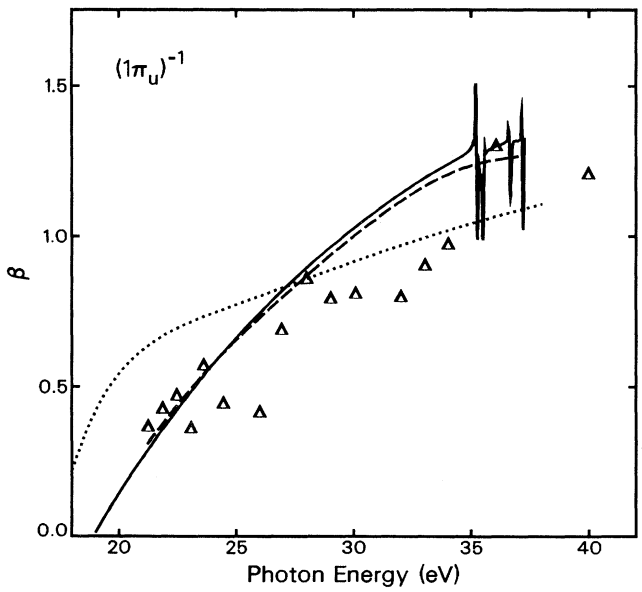

FIG. 4. Photoelectron asymmetry parameter in the $(1\pi_u)^{-1}$ channel. ——, MCFCHF four-channel mixed form; — — —, RPA mixed form; · · ·, SCFCHF mixed form; △, experimental data of Marr *et al.* [37].

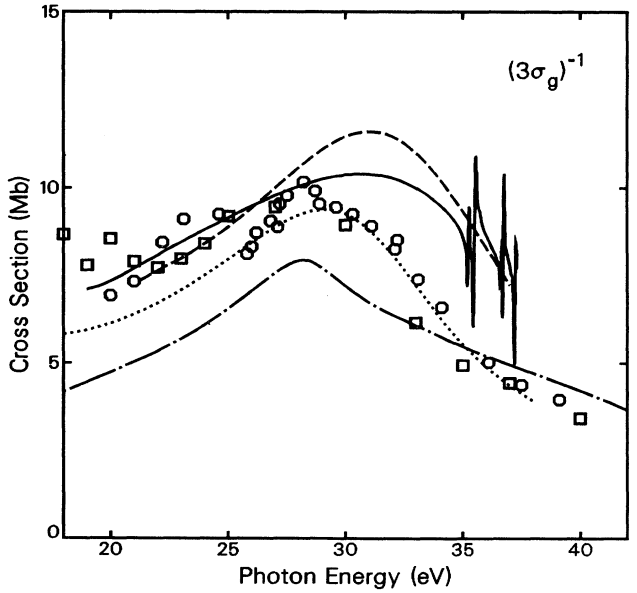

FIG. 5. Photoionization cross section in the $(3\sigma_g)^{-1}$ channel. ——, MCFCHF four-channel mixed form; — — —, RPA mixed form; · · ·, SCFCHF mixed form; —·—·—, RPA results of Swanstrøm *et al.* [5]; □, experimental data from Hamnett, Stoll, and Brion [8]; ○, experimental data of Plummer *et al.* [9].

in the one-particle basis set, the approximations inherent in the treatment of the continuum with the Stieltjes-Tchebycheff moment theory, and the approximate method used to separate the photoionization oscillator strength into partial channels. Swanstrøm *et al.* [5] also performed more sophisticated MCRPA's where additional initial and final-state correlations were included. The differences between the RPA and MCRPA calculations of Swanstrøm *et al.* [5] were of the same order of magnitude as the differences between the accurate RPA results presented here and the RPA results of Swanstrøm *et al.* [5]. This indicates that a more accurate treatment of the continuum part of the problem than that used by Swanstrøm *et al.* [5] is needed before one can assess the importance of various correlation effects.

The photoelectron asymmetry parameters plotted in Fig. 6 for the $(3\sigma_g)^{-1}$ channel show that all three theoretical results are in good agreement with each other. The significant deviation between theory and experimental data of Marr *et al.* [37] and Southworth *et al.* [10] near a photon energy of 22 eV is due to autoionization leading to the $C\,^2\Sigma_u^+$ state of N_2^+ which is not included in any of the present calculations [9].

In Figs. 7 and 8 we present the cross sections and asymmetry parameters for photoionization leading to the $(2\sigma_u)^{-1}$ state of N_2^+. All three of the present calculations for the total cross sections are in fair agreement with the experimental data of Hamnett, Stoll, and Brion [8] and Plummer *et al.* [9] although the SCFCHF seems to be in somewhat better agreement with the experiments. The agreement between the present RPA and the previously reported RPA is fairly good in terms of the

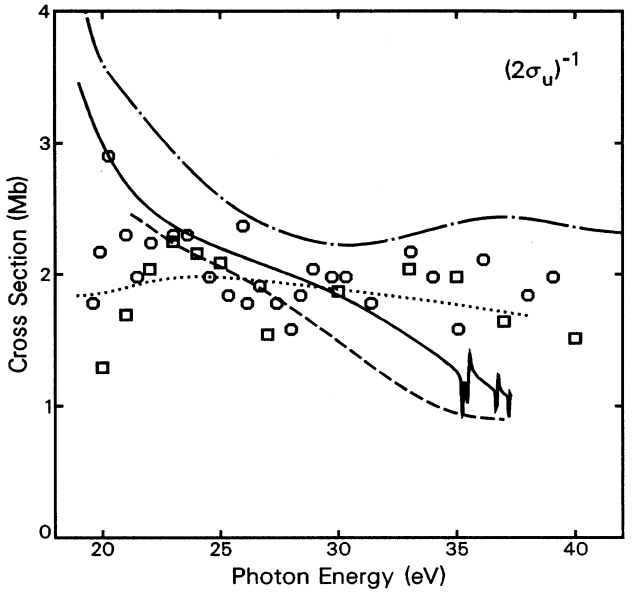

FIG. 7. Photoionization cross section in the $(2\sigma_u)^{-1}$ channel. ——, MCFCHF four-channel mixed form; — — —, RPA mixed form; · · ·, SCFCHF mixed form; —·—·—·, RPA results of Swanstrøm *et al.* [5]; □, experimental data from Hamnett, Stoll, and Brion [8]; ○, experimental data of Plummer *et al.* [9].

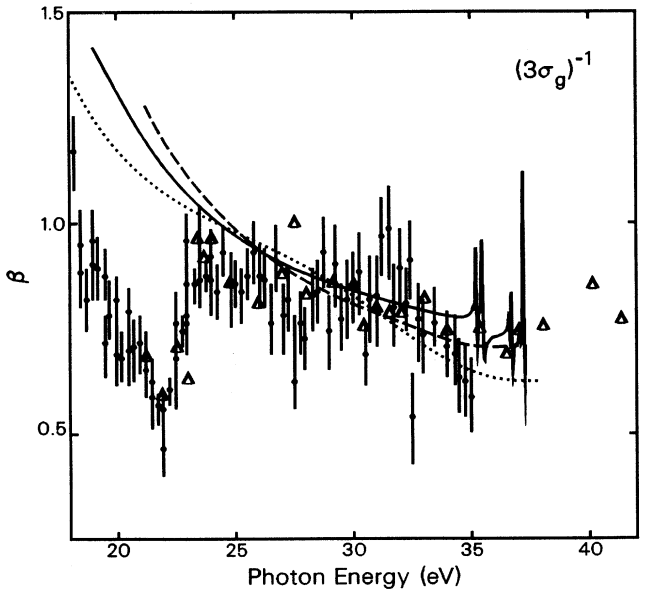

FIG. 6. Photoelectron asymmetry parameter in the $(3\sigma_g)^{-1}$ channel. ——, MCFCHF four-channel mixed form; — — —, RPA mixed form; · · ·, SCFCHF mixed form; △, experimental data of Marr *et al.* [37]; ●, experimental data of Southworth *et al.* [10].

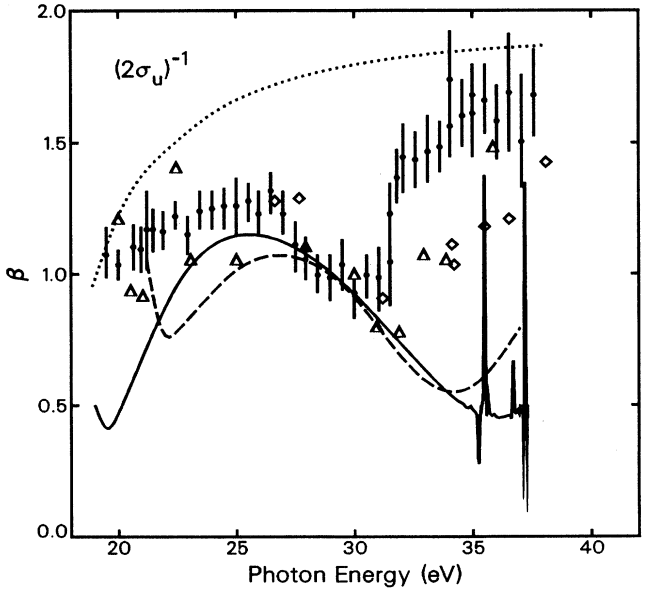

FIG. 8. Photoelectron asymmetry parameter in the $(2\sigma_u)^{-1}$ channel. ——, MCFCHF four-channel mixed form; — — —, RPA mixed form; · · ·, SCFCHF mixed form; △, experimental data of Marr *et al.* [37]; ●, experimental data of Southworth *et al.* [10]; ◇, experimental data of Adam *et al.* [39].

absolute differences in the cross sections with differences of less than 2 Mb at all energies. The computed photoelectron asymmetry parameters for the coupled-channel calculations show a large dip near a photon energy of 35 eV, which is due to the interchannel coupling with the shape resonance in the $(3\sigma_g)^{-1}$ channel [1, 18, 38]. Somewhat better agreement between theory and the experimental data of Marr *et al.* [37] and Adam *et al.* [39] was obtained in an earlier MCFCHF calculation in which only the coupling between the $(3\sigma_g)^{-1}$ and $(2\sigma_u)^{-1}$ channels was included (not shown) [1,18]. The discrepancy between the earlier experimental data and the data of Southworth *et al.* [10] has yet to be satisfactorily explained. One difference between these data is that the Southworth *et al.* [10] cross sections were vibrationally resolved, whereas the data of Marr *et al.* [37] and Adam *et al.* [39] were averaged over the final vibrational states. In earlier calculations [1], we have shown that the differences between a vibrationally resolved and a vibrationally averaged cross section does not seem to be large enough to explain the discrepancies between these sets of experimental data. The asymmetry parameters given in Fig. 8 are another indication that the four-channel MCFCHF and RPA calculations yield a shape resonance in the $(3\sigma_g)^{-1}$ channel, which is too broad and at too high of an energy when compared to the experimental data.

In Figs. 9 and 10 we consider the photoionization cross sections and asymmetry parameters for $(3\sigma_g)^{-1}$ ionization in the energy region below the threshold for the production of the $(2\sigma_u)^{-1}$ state of N_2^+. The resonances found in this energy region are part of the series of autoionization states observed by Hopfield [40]. The agreement between the theoretical cross sections and the experimental data of Plummer *et al.* [9], Hamnett, Stoll, and Brion [8], and Morin [41] is fairly good with the positions off by less than 0.1 eV and with similar intensity patterns. In the experimental data of Plummer *et al.* [9] there is some structure that is in part due to the various different final vibrational states. In the present calculation we have used only the fixed-nuclei approximation which will lead to only one set of autoionization levels without the vibrational progressions. The photoelectron asymmetry parameters given in Fig. 10 also show a pronounced autoionization structure which is in fair agreement with the experimental data of West *et al.* [11]. However, due to the limited resolution of the experimental data, a detailed comparison is not possible. In Fig. 11 the partial-channel cross sections for the $(3\sigma_g)^{-1}$ ionization in this energy region are given. This figure indicates that most of the intensity for these resonant states comes from the ionization process with $\Delta m=0$, where the final-state wave function including continuum and target electrons has a total symmetry $^2\Sigma_u^+$ (i.e., the $k\sigma_u$ channel). The $\Delta m=1$ channel (i.e., the $k\pi_u$ channel) is seen to have a small window resonance in the same energy region. The four peaks at 17.20, 17.55, 17.90, and 18.05 eV seen in Figs. 9 and 11 are in the region where the $n=3$ and 4 Rydberg levels leading to the $(2\sigma_u)^{-1}$ state should be. Thus the first two peaks are probably due to linear combinations of the $2\sigma_u \rightarrow 3s\sigma_g$ and $2\sigma_u \rightarrow 3d\sigma_g$ Rydberg states. The second two peaks would then be the corresponding $n=4$ states.

In Figs. 9 and 10 we have also compared our results to the MQDT results of Raoult *et al.* [3]. In the MQDT re-

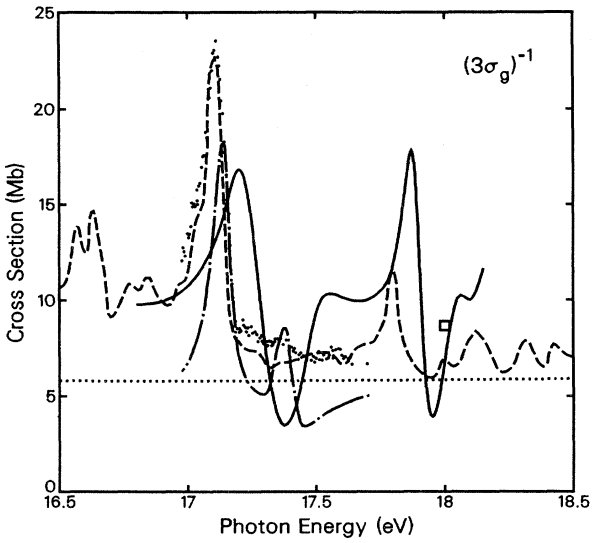

FIG. 9. Photoionization cross section in the $(3\sigma_g)^{-1}$ channel in the region of autoionization. ——, MCFCHF four-channel mixed form; · · ·, SCFCHF mixed form; —·—·—·, MQDT results of Raoult *et al.* [3]; ●, experimental data of Morin; □, experimental data from Hamnett, Stoll, and Brion [8]; — — —, relative experimental data of Plummer *et al.* [9] which has been scaled to approximately agree with the absolute data of Morin [41].

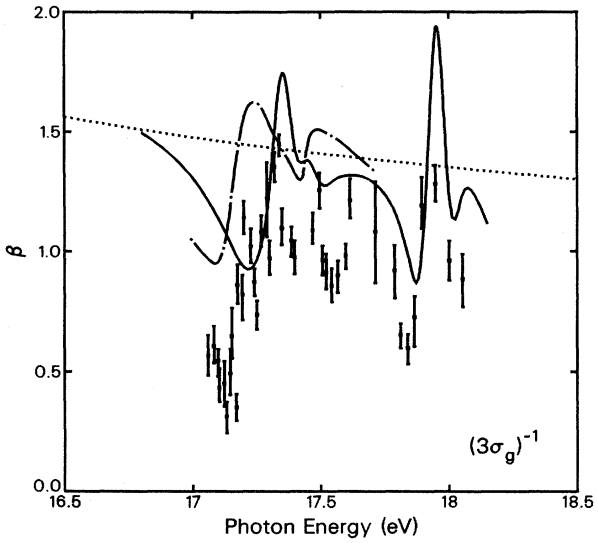

FIG. 10. Photoelectron asymmetry parameter in the $(3\sigma_g)^{-1}$ channel in the region of autoionization: ——, MCFCHF four-channel mixed form; · · ·, SCFCHF mixed form; —·—·—·, MQDT results of Raoult *et al.* [3]; ■, experimental data of West *et al.* [11].

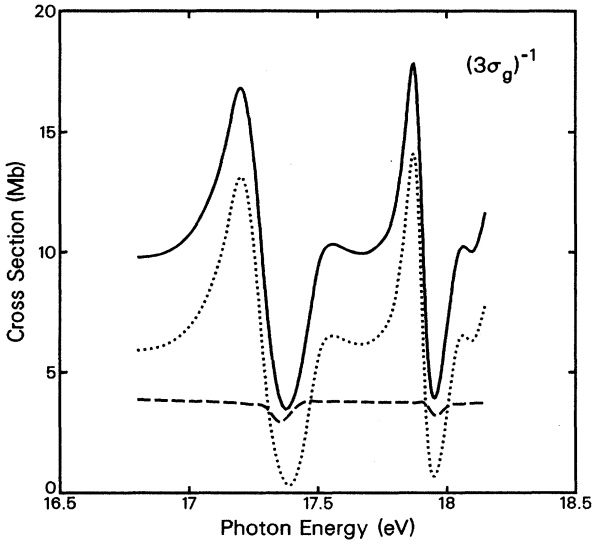

FIG. 11. Partial photoionization cross section in the MCFCHF four-channel mixed form for the $(3\sigma_g)^{-1}$ channel in the region of autoionization. ——, total cross section; · · ·, $3\sigma_g \rightarrow k\sigma_u$ channel; — — —, $3\sigma_g \rightarrow k\pi_u$ channel.

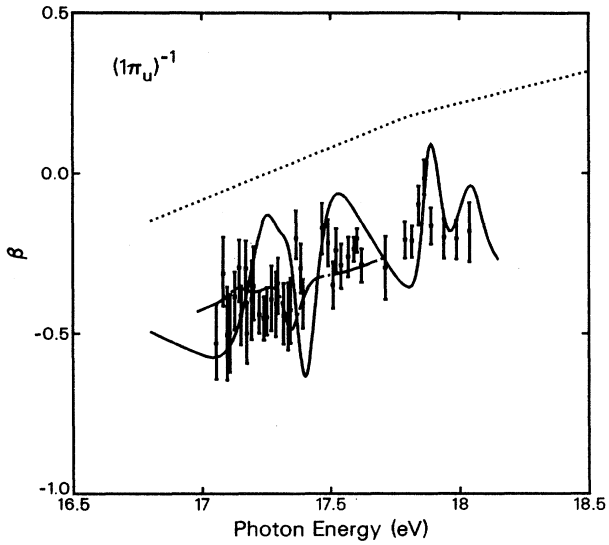

FIG. 13. Photoelectron asymmetry parameter in the $(1\pi_u)^{-1}$ channel in the region of autoionization: ——, MCFCHF four-channel mixed form; · · ·, SCFCHF mixed form; —·—·—·, MQDT results of Raoult *et al.* [3]; ■, experimental data of West *et al.* [11].

sult the resonance at 17.40 eV is somewhat closer to the resonance at 17.15 eV than to the next member of the series which in the MCFCHF results appears at 17.90 eV. This is in contrast to the MCFCHF result where the peak at 17.55 eV appears as a shoulder of the peak at 17.90 eV. An additional difference between the MQDT and MCFCHF results is that the resonance in the $3\sigma_g \rightarrow k\pi_u$ channel is a pure window resonance in the MCFCHF approximation, and it has a quite different shape in the MQDT [3]. This difference is not readily apparent in the total cross sections given in Fig. 9 since the $3\sigma_g \rightarrow k\pi_u$ channel makes a minor contribution to the total cross section. In comparing either theoretical result to the ex-

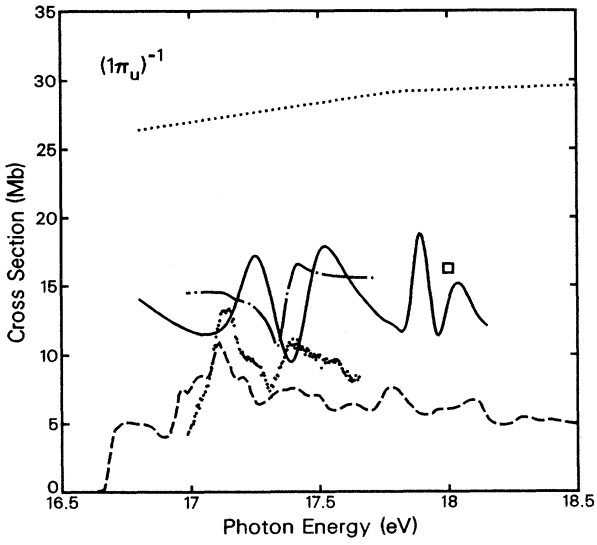

FIG. 12. Photoionization cross section in the $(1\pi_u)^{-1}$ channel in the region of autoionization: ——, MCFCHF four-channel mixed form; · · ·, SCFCHF mixed form; —·—·—·, MQDT results of Raoult *et al.* [3]; ●, experimental data of Morin; □, experimental data from Hamnett, Stoll, and Brion [8]; — — —, relative experimental data of Plummer *et al.* [9] which has been scaled to approximately agree with the absolute data of Morin [41].

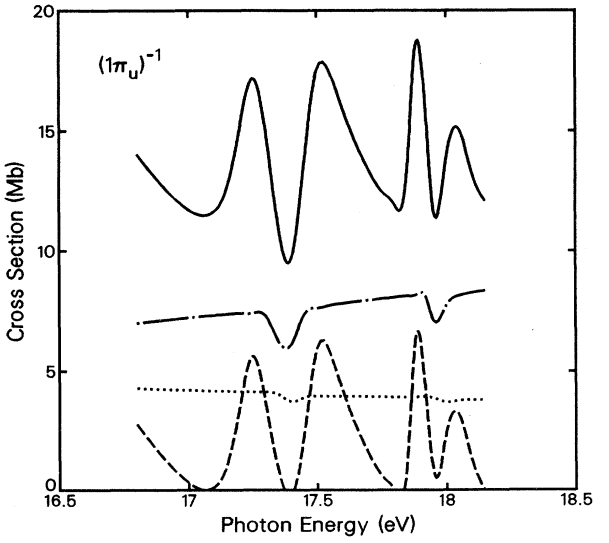

FIG. 14. Partial photoionization cross section in the MCFCHF four-channel mixed form for the $(1\pi_u)^{-1}$ channel in the region of autoionization. ——, total cross section; · · ·, $1\pi_u \rightarrow k\sigma_g$ channel; — — —, $1\pi_u \rightarrow k\pi_g$ channel; —·—·—·, $1\pi_u \rightarrow k\delta_g$ channel.

perimental data, it is unclear which feature in the experimental data corresponds to the resonance which occurs at 17.40 eV in the MQDT and at 17.55 eV in the MCFCHF result. The MCFCHF results presented here would suggest that the feature which appears as a window resonance in the data of Plummer *et al.* [9] at 17.6 eV is a dip between two resonant peaks, one being the resonance in the $3\sigma_g \rightarrow k\sigma_u$ channel found at 17.55 eV in the MCFCHF calculation and the other being a resonance at 17.65 eV due to a different vibrational progression [3].

The cross sections and asymmetry parameters for the $(1\pi_u)^{-1}$ channel in the region of the Hopfield series are given in Figs. 12–14. Again we can see a reasonable correspondence between theory and experiment for the $n=3$ and 4 Hopfield transitions. The theory correctly shows that the intensities of all four peaks are roughly the same, whereas in the $(3\sigma_g)^{-1}$ channel there was a definite alternation of intensity. The agreement with the experimental asymmetry parameters shown in Fig. 13 is fairly good. The experimental data of West *et al.* [11] shows a fair amount of structure, which seems to be in reasonable agreement with the present theory in both the amplitude of the oscillations and in their locations. The partial cross sections for this channel are shown in Fig. 14, where we can see that there are window resonances in both of the $\Delta m=1$ channels (i.e., the $k\sigma_g$ and $k\delta_g$ channels) but most of the variation in the intensity comes from the $\Delta m=0$ channel (i.e., the $k\pi_g$ channel). This result is in contrast to the MQDT result of Raoult *et al.* [3] in which the structure in the cross section is only due to the window resonance in the $\Delta m=1$ channel with very little contribution from the $\Delta m=0$ channel. The larger discrepancies between the MQDT and MCFCHF results found in the $(1\pi_u)^{-1}$ channel can be attributed to the use of a modified potential in the $1\pi_u \rightarrow k\pi_g$ ionization channel in the MQDT calculation but not in the MCFCHF calculation. As noted in the Introduction, this procedure was necessary to remove a strong valence transition from the continuum in any SCFCHF calculation such as the one used to obtain the MQDT parameters [3].

IV. CONCLUSIONS

We have found that the mixed form of the MCFCHF cross section gives a result that is qualitatively very similar to the RPA result. Thus there seems to be little motivation for using the RPA formalism considering that it is more computationally intensive than the MCFCHF calculation and that it does not have the correct ionization thresholds so that one cannot study autoionization with the RPA.

Comparing the four-channel MCFCHF and SCFCHF calculations, we see that the MCFCHF method has qualitatively improved the calculation by yielding autoionization resonances, by dramatically reducing the intensity in the $1\pi_u \rightarrow k\pi_g$ continuum channel, and by including the important interchannel coupling effects which lead to the structure in the $(2\sigma_u)^{-1}$ photoelectron asymmetry parameters near 33 eV. Although the qualitative features of the computed cross sections are improved by considering the effects of the interchannel coupling, quantitative agreement is made worse in some channels as exemplified by the fact that the SCFCHF results give better agreement with the experiments for the width and position of the resonance in the $(3\sigma_g)^{-1}$ ionization channel.

The MCFCHF method gives a good qualitative representation of the autoionization resonances in the Hopfield series, although the details of the cross sections do not yet agree with the experimental data. We are currently developing methods which will allow a more detailed study of the position and qualitative nature of the autoionizing states.

ACKNOWLEDGMENTS

This material is based on work supported in part by the National Science Foundation under Grant No. CHE-83-51414 and in part by the Robert A. Welch Foundation (Houston, TX) under Grant No. A-1020. Support from the Alfred P. Sloan Foundation and from the Camille and Henry Dreyfus Foundation is also gratefully acknowledged. Computations for this work were in part carried out at the Pittsburgh Supercomputer Center and at the Texas A&M Supercomputer Center.

[1] B. Basden and R. R. Lucchese, Phys. Rev. A **37**, 89 (1988).
[2] R. R. Lucchese, G. Raseev, and V. McKoy, Phys. Rev. A **25**, 2572 (1982).
[3] M. Raoult, H. Le Rouzo, G. Raseev, and H. Lefebvre-Brion, J. Phys. B **16**, 4601 (1983).
[4] T. N. Rescigno, C. F. Bender, B. V. McKoy, and P. W. Langhoff, J. Chem. Phys. **68**, 970 (1978).
[5] P. Swanstrøm, J. T. Golab, D. L. Yeager, and J. A. Nichols, Chem. Phys. **110**, 339 (1986).
[6] G. R. J. Williams and P. W. Langhoff, Chem. Phys. Lett. **78**, 21 (1981).
[7] S. Yabushita and C. W. McCurdy, Phys. Rev. A **36**, 3146 (1987).
[8] A. Hamnett, W. Stoll, and C. E. Brion, J. Electron Spectrosc. Relat. Phenom. **8**, 367 (1976).
[9] E. W. Plummer, T. Gustafsson, W. Gudat, and D. E. Eastman, Phys. Rev. A **15**, 2339 (1977).
[10] S. H. Southworth, A. C. Parr, J. E. Hardis, and J. L. Dehmer, Phys. Rev. A **33**, 1020 (1986).
[11] J. B. West, K. Codling, A. C. Parr, D. L. Ederer, B. E. Cole, R. Stockbauer, and J. L. Dehmer, J. Phys. B **14**, 1791 (1981).
[12] T. N. Rescigno, A. Gerwer, B. V. McKoy, and P. W. Langhoff, Chem. Phys. Lett. **66**, 116 (1979).
[13] R. R. Lucchese, J. Chem. Phys. **92**, 4203 (1990).
[14] C. W. McCurdy, Jr., T. N. Rescigno, D. L. Yeager, and V. McKoy, in *Methods of Electronic Structure Theory*, edited by H. F. Schaefer III (Plenum, New York, 1977), Vol. 3, p. 339.
[15] A. Dalgarno and G. A. Victor, Proc. R. Soc. London, Ser. A **291** 291 (1966).
[16] R. R. Lucchese, K. Takatsuka, and V. McKoy, Phys. Rep. **131**, 147 (1986).
[17] B. Basden and R. R. Lucchese, J. Comput. Phys. **77**, 524

(1988).
[18] B. Basden and R. R. Lucchese, Phys. Rev. A **34**, 5158 (1986).
[19] I. Cacelli, V. Carravetta, and R. Moccia, Chem. Phys. **120**, 51 (1988).
[20] I. Cacelli, V. Carravetta, R. Moccia, and A. Rizzo, J. Phys. Chem. **92**, 979 (1988).
[21] R. K. Nesbet, *Variational Methods in Electron-Atom Scattering Theory* (Plenum, New York, 1980).
[22] R. R. Lucchese, Phys. Rev. A **33**, 1626 (1986).
[23] J. D. Weeks, A. Hazi, and S. A. Rice, in *Advances in Chemical Physics,* edited by I. Prigogine and S. A. Rice (Wiley Interscience, New York, 1969), Vol. XVI, p. 283.
[24] K. Takatsuka and V. McKoy, Phys. Rev. A **23**, 2352 (1981).
[25] R. R. Lucchese and V. McKoy, Phys. Rev. A **28**, 1382 (1983).
[26] A. E. Hansen, Mol. Phys. **13**, 425 (1967).
[27] J. C. Tully, R. S. Berry, and B. J. Dalton, Phys. Rev. **176**, 95 (1968).
[28] A. E. Hansen and T. D. Bouman, Chem. Phys. Lett. **45**, 326 (1977).
[29] B. Apagyi, P. Levay, and K. Ladanyi, Phys. Rev. A **37**, 4577 (1988).
[30] W. Huo, M. A. P. Lima, T. L. Gibson, and V. McKoy, Phys. Rev. A **36**, 1642 (1987).
[31] T. N. Rescigno and B. I. Schneider, J. Phys. B **21**, L691 (1988).
[32] R. E. Stratmann and R. R. Lucchese (unpublished).
[33] A. Rizzo, R. L. Graham, and D. L. Yeager, J. Chem. Phys. **89**, 1533 (1988).
[34] K. P. Huber and G. Herzberg, *Molecular Spectra and Molecular Structure IV. Constants of Diatomic Molecules* (Van Nostrand Reinhold, New York, 1979).
[35] S. Krummacher, V. Schmidt, and F. Wuilleumier, J. Phys. B **13**, 3993 (1980).
[36] P. W. Langhoff, S. R. Langhoff, T. N. Rescigno, J. Schirmer, L. S. Cederbaum, W. Domcke, and W. Von Niessen, Chem. Phys. **58**, 71 (1981).
[37] G. V. Marr, J. M. Morton, R. M. Holmes, and D. G. McCoy, J. Phys. B **12**, 43 (1979).
[38] J. A. Stephens and D. Dill, Phys. Rev. A **31**, 1968 (1985).
[39] M. Y. Adam, P. Morin, P. Lablanquie, and I. Nenner (unpublished).
[40] J. J. Hopfield, Phys. Rev. **36**, 789 (1930).
[41] P. Morin, Ph.D. thesis, Universite de Paris-Sud, 1983.